Composites Science and Technology 227 (2022) 109607

Contents lists available at ScienceDirect

Composites Science and Technology

journal homepage: www.elsevier.com/locate/compscitech

A microstructure-based model of transport parameters and sound absorption for woven fabrics

Wei He [a,d], Xiangjun Peng [a,d], Fengxian Xin [a,d,*], Tian Jian Lu [b,c,**]

[a] State Key Laboratory for Strength and Vibration of Mechanical Structures, Xi'an Jiaotong University, Xi'an, 710049, PR China
[b] State Key Laboratory of Mechanics and Control of Mechanical Structures, Nanjing University of Aeronautics and Astronautics, Nanjing, 210016, PR China
[c] MIIT Key Laboratory of Multi-functional Lightweight Materials and Structures, Nanjing University of Aeronautics and Astronautics, Nanjing, 210016, PR China
[d] MOE Key Laboratory for Multifunctional Materials and Structures, Xi'an Jiaotong University, Xi'an, 710049, PR China

ARTICLE INFO

Keywords:
Porous materials
Woven fabrics
Microstructure-based model
Transport parameters
Sound absorption

ABSTRACT

A microstructure-based model is proposed to describe the transport parameters and sound absorption performance of idealized periodic woven fabrics. With proper hypotheses and simplifications, transport parameters, including permeability, tortuosity, viscous characteristic length and thermal characteristic length, are explicitly expressed as functions of fiber diameter and porosity. The unknown control coefficients introduced in the analytical model are fitted by performing multiscale numerical simulations over the representative unit cells. Subsequently, these transport parameters are submitted into the well-established Johnson-Champoux-Allard (JCA) model of porous media to calculate the acoustic impedance and sound absorption coefficient of the woven fabric. Compared with the corresponding transport parameters of a non-crimp fabric, the tortuosity is enlarged and viscous characteristic length decreases significantly, while the viscous permeability and thermal characteristic length remain almost unchanged, resulting in slightly improved performance in sound absorption. The fiber diameter, porosity, and thickness of a woven fabric comprehensively determine its capability to absorb sound. For enhanced energy dissipation (and hence sound absorption) via viscous-thermal boundary layers on fiber surfaces, the fiber diameter and porosity should be selected from an appropriate range such that the characteristic pore size of the woven fabric lies in the order of submillimeter. With the increase of sheet thickness, the sound absorption coefficient in the low frequency band is significantly improved.

1. Introduction

Woven fabrics are typically produced by periodically interlacing two or more sets of fibers at purposely selected angles and spacings. With attractive properties such as high specific strength, Kevlar woven fabrics are widely used to construct body armors and seat belts [1,2]; glass and carbon woven fabrics are integrated in armor panels for enhanced impact resistance [3–5]; while, with large specific surface area, copper woven fabrics are found to exhibit superior heat dissipation capability [6–8]. In addition to engineering applications, in daily life, as woven fabrics are the important raw material for clothes, their air permeability seriously affects wearing comfort [9]. Further, strain sensors made of graphene oxide woven fabrics simultaneously possess good sensitivity and stretchability, enabling applications in wearable electronics to monitor human activities [10].

As a typical kind of porous materials, woven fabrics can also effectively absorb sound. When a sound wave is incident, the fiber surface retards the movement of air particles and converts a portion of acoustic energy into useless heat via thermo-viscous dissipation. It has been well established that the macroscopic sound absorption performance of porous materials is closely related to morphological details at pore scale. Compared to a stochastic cellular foam or fibrous material, the morphology of a woven fabric can be conveniently adjusted by changing the weaving type and geometrical parameters. In other words, the ability of the woven fabric to absorb sound can be precisely regulated according to practical needs.

The sound absorption performance of woven fabrics has been evaluated using a variety of approaches. Built upon the equivalent circuit

* Corresponding author. State Key Laboratory for Strength and Vibration of Mechanical Structures, Xi'an Jiaotong University, Xi'an, 710049, PR China.
** Corresponding author. State Key Laboratory of Mechanics and Control of Mechanical Structures, Nanjing University of Aeronautics and Astronautics, Nanjing, 210016, PR China.
E-mail addresses: fengxian.xin@gmail.com (F. Xin), tjlu@nuaa.edu.cn (T.J. Lu).

https://doi.org/10.1016/j.compscitech.2022.109607
Received 24 February 2022; Received in revised form 17 June 2022; Accepted 20 June 2022
Available online 24 June 2022

method and the impedance transfer matrix method, an approximate theoretical model was developed to estimate how woven fabric sheets attenuate noise [11]. After experimentally measuring the sound absorption coefficient of woven fabrics, its functional relationship with key physical parameters was fitted via multiple regression analysis [12]. Compared to air, the solid frame of fabrics is sufficiently stiff and motionless, hence the porous material can be substituted by a layer of equivalent fluid [13,14]. The equivalent fluid density and bulk modulus of porous materials involve several transport parameters, such as permeability, tortuosity, viscous characteristic length and thermal characteristic length. With the woven fabric taken as a micro-perforated plate, a theoretical model was established to approximately investigate its transport parameters and sound absorption [15]. Numerically simulated transport parameters of woven fabrics were fitted and then substituted into the equivalent fluid model of porous media to calculate sound absorption [16]. However, despite all these efforts, how the important morphological parameters of a woven fabric sheet, e.g., porosity, fiber diameter and sheet thickness, affects its transport parameters and sound absorption is not yet systematically quantified, especially from theoretical point of view.

The present study aims to develop a microstructure-based analytical model of transport parameters and sound absorption for plain woven fabrics. To evaluate the influence of the weaving process, transport parameters and sound absorption of non-crimp fabrics are also explored by using the same method. Based on the morphology of representative unit cells, transport parameters of fabrics are explicitly expressed as functions of geometrical parameters. The unknown control coefficients in the analytical model are then fitted according to multiscale numerical simulation results. For validation, the transport parameters and sound absorption coefficient of a 3D printed micro-lattice are calculated and compared with existing numerical and experimental results [17]. Finally, the transport parameters are substituted into the equivalent fluid model to quantify how sound absorption of a woven fabric sheet is influenced by key morphological parameters such as porosity, fiber diameter, and sheet thickness.

2. Analytical model

2.1. Geometrical properties of woven fabrics

As shown in Fig. 1(a)-(c), multilayer plain woven fabric sheets are stacked from bottom to up. For simplicity, warp and weft fibers are perfectly circular and have the same diameter, and no offset is allowed between adjacent layers. The transverse and longitudinal spacing of fibers are set to be equal, thus the pore morphology viewed from top to bottom is like a square. To reveal the influence of the weaving process on transport parameters and sound absorption of woven fabrics, non-crimp fabrics, as presented in Fig. 1(d)–(f), is also studied: circular fibers in each layer of the non-crimp fabric are arranged in parallel, and the ply angle of two adjacent layers is rotated by 90°.

Due to periodicity, representative unit cells of both woven and non-crimp fabrics, as presented in Fig. 2, are chosen to simplify subsequent analysis. Let d and l denote fiber diameter and spacing, respectively. For woven fabrics, the axis of each fiber at the bend is transited smoothly through a segment of circular arc.

Fig. 3 displays the specific geometric characteristics of plain weave type. With the line BC passing through the coordinate origin, its governing equation is assumed to be:

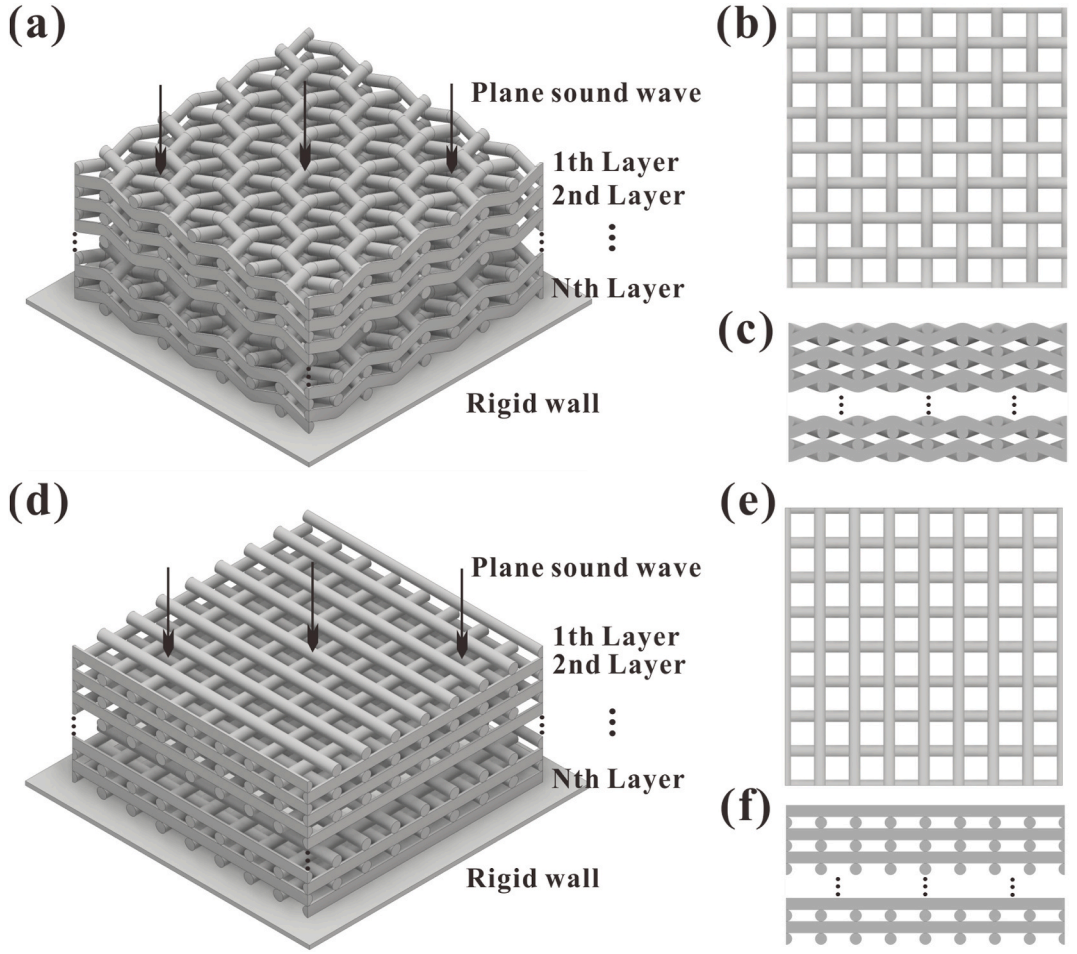

Fig. 1. Schematic of (a) woven and (d) non-crimp fabrics. (b) and (e) are top views of (a) and (d) while (c) and (f) are side views of (a) and (d), respectively.

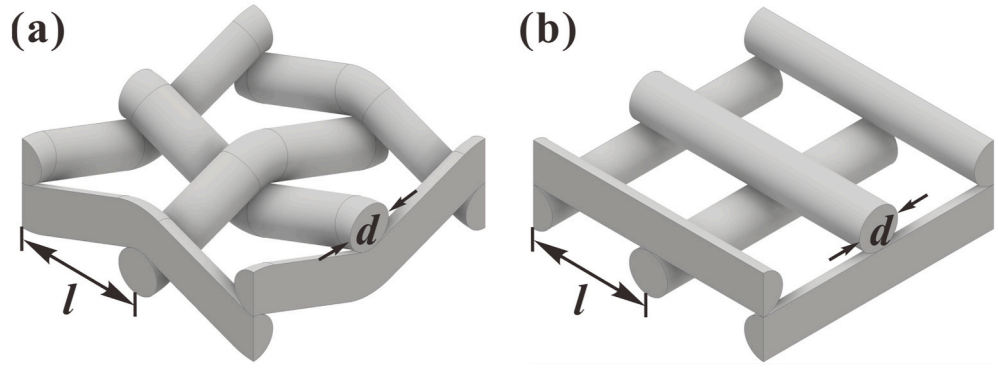

Fig. 2. Representative unit cell of (a) woven and (b) non-crimp fabrics.

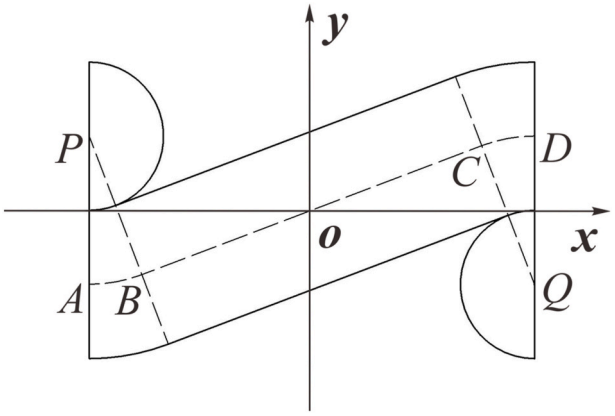

Fig. 3. Specific geometric characteristics of plain weave type.

$$y = mx \tag{1}$$

where m is the slope of line BC. The arc AB is part of the circumference of a circle, centered at point $P(-l/2, d/2)$ with a radius d, which is governed by:

$$\left(x+\frac{l}{2}\right)^2+\left(y-\frac{d}{2}\right)^2=d^2 \tag{2}$$

Substitution of Eq. (1) into Eq. (2) yields:

$$4\left(m^2+1\right)x^2+4(l-dm)x+l^2-3d^2=0 \tag{3}$$

Since line BC is tangent to arc AB, Eq. (3) has exactly one solution, which requires:

$$\left(4d^2-l^2\right)m^2-2dlm+3d^2=0 \tag{4}$$

As the slope of line BC is greater than 0, the solution of m can be expressed as:

$$m=\begin{cases}\dfrac{dl-2d\sqrt{l^2-3d^2}}{4d^2-l^2}, l>2d\\ \dfrac{3}{4}, l=2d\\ \dfrac{dl+2d\sqrt{l^2-3d^2}}{4d^2-l^2}, 2d>l\geq\sqrt{3}d\end{cases} \tag{5}$$

For the representative unit cell of woven fabrics shown in Fig. 2(a), the length of each fiber s is given by:

$$s=2\left(\frac{l}{\cos\theta}-2d\tan\theta+2d\theta\right)=\frac{2l}{\cos\theta}-4d\tan\theta+4d\theta \tag{6}$$

where $\theta=\arctan(m)$ is the central angle corresponding to arc AB (and CD). Then, the volume of solid frame V_s and the solid-fluid interface area S are determined by:

$$V_s=\pi d^2 s \tag{7}$$

$$S=4\pi ds \tag{8}$$

Correspondingly, for non-crimp fabrics of Fig. 2(b):

$$V_s=2\pi d^2 l \tag{9}$$

$$S=8\pi dl \tag{10}$$

For a porous material, the porosity φ is defined as the ratio of interconnected air volume to its total volume. Since both woven and non-crimp fabrics can be regarded as a periodic array of representative unit cells, the porosity is equal to that of representative unit cell:

$$\varphi=\frac{V_a}{V}=1-\frac{V_s}{V} \tag{11}$$

where V_a is the volume filled with air and $V=8l^2d$ is the volume of representative unit cell. For woven fabrics, to avoid fiber overlapping, l should be larger than $\sqrt{3}d$ and hence the porosity is always larger than 0.4517. Similarly, for non-crimp fabrics, l should be larger than d and hence the porosity is always larger than 0.2146.

2.2. The equivalent fluid model of porous materials

When the incident harmonic sound wave has low intensity, the fluid velocity $\mathbf{u}=\mathbf{u}(\mathbf{r})e^{-j\omega t}$ within the pores of a porous material is linearly related to sound pressure $p=p(\mathbf{r})e^{-j\omega t}$, expressed as [13,18]:

$$\rho_0\alpha(\omega)\frac{\partial\langle\mathbf{u}\rangle}{\partial t}=-\nabla\langle p\rangle \tag{12}$$

$$\varphi\langle\mathbf{u}\rangle=-\frac{k(\omega)}{\mu}\nabla\langle p\rangle \tag{13}$$

where $\mathbf{r}$ is the position vector of air particles, j is the is the imaginary unit, $\omega=2\pi f$ is the angular frequency, f is the frequency of incident sound wave, t is the time variable, ρ_0 is the density of air, $\alpha(\omega)$ is the dynamic tortuosity, $k(\omega)$ is the dynamic viscous permeability, μ is the viscosity coefficient of air, and the symbol $\langle\ \rangle$ denotes the average operator over the fluid domain. The dynamic tortuosity is related to dynamic viscous permeability via:

$$\alpha(\omega)=-\frac{\mu\varphi}{j\omega\rho_0 k(\omega)} \tag{14}$$

At the low frequency limit, namely $\omega\to0$, the dynamic viscous permeability $k(\omega)$ approaches to the static viscous permeability k_0:

$$\lim_{\omega\to 0} k(\omega) = k_0 \tag{15}$$

In this case, Eq. (13) is simplified to $\varphi\langle \mathbf{u}\rangle = -k_0\nabla\langle p\rangle/\mu$, which is the definition of the classical Darcy's law. While, at the high frequency limit ($\omega\to\infty$), the dynamic viscous permeability $k(\omega)$ is approximately replaced by the following asymptotic expression [13]:

$$k(\omega) = \frac{\mu\varphi}{-j\rho_0\omega\alpha_\infty}\left[1-(1+j)\frac{\delta}{\Lambda}\right] \tag{16}$$

where $\delta = \sqrt{2\mu/(\rho_0\omega)}$ is the viscous skin depth and Λ is the viscous characteristic length of porous material. According to the above two limit cases, it is assumed that the dynamic viscous permeability in the medium frequency range is approximately given by Refs. [13,18]:

$$k(\omega) = \frac{k_0}{\sqrt{1-j\frac{M\omega\rho_0 k_0\alpha_\infty}{2\mu\varphi}} - j\frac{\omega\rho_0 k_0\alpha_\infty}{\mu\varphi}} \tag{17}$$

where $M = (8\alpha_\infty k_0)/(\varphi\Lambda^2)$ is the dimensionless viscous shape factor.

The equivalent fluid density of a porous material is defined as:

$$\widetilde{\rho}(\omega) = \rho_0\alpha(\omega) \tag{18}$$

It follows that Eq. (12) can be rewritten as:

$$\widetilde{\rho}(\omega)\frac{\partial\langle \mathbf{u}\rangle}{\partial t} = -\nabla\langle p\rangle \tag{19}$$

The governing equation of a sound wave propagating in air is given by:

$$\rho_0\frac{\partial\langle \mathbf{u}\rangle}{\partial t} = -\nabla\langle p\rangle \tag{20}$$

Note that Eqs. (19) and (20) have the same form. Upon substituting (14) and (17) into (18), the effective density is simplified to:

$$\widetilde{\rho}(\omega) = \rho_0\alpha_\infty\left[1+\frac{\mu\varphi}{j\omega\rho_0 k_0\alpha_\infty}\sqrt{1+j\frac{4\alpha_\infty^2 k_0^2\omega\rho_0}{\mu\varphi^2\Lambda^2}}\right] \tag{21}$$

Similarly, under the excitation of sound wave, the excess temperature of air T in the pores is also linearly related to sound pressure p, as [18]:

$$\varphi\langle T\rangle = \frac{k'(\omega)}{\kappa}\frac{\partial\langle p\rangle}{\partial t} \tag{22}$$

where $k'(\omega)$ is the dynamic thermal permeability, and κ is the thermal conductivity of air. The compression response of air in a porous material is given by Ref. [18]:

$$\frac{\beta(\omega)}{K}\frac{\partial\langle p\rangle}{\partial t} = -\nabla\cdot\langle \mathbf{u}\rangle \tag{23}$$

where $\beta(\omega)$ is the scaled dynamic compressibility, $K = \gamma P_0$ is the bulk modulus of air, γ is the specific heat ratio of air, and P_0 is the ambient pressure. $\beta(\omega)$ can be written as a function of $k'(\omega)$ as [18]:

$$\beta(\omega) = \gamma + (\gamma-1)\frac{j\omega}{\mu'\varphi}k'(\omega) \tag{24}$$

where $\mu' = \kappa/(\rho_0 C_p)$, and C_p is the specific heat capacity at constant pressure.

When the frequency of sound wave tends to 0, the dynamic thermal permeability $k'(\omega)$ approaches to the static thermal permeability k_0', namely [18]:

$$\lim_{\omega\to 0} k'(\omega) = k_0' \tag{25}$$

In the high frequency range, $k'(\omega)$ can be approximately expressed as [14,18]:

$$k'(\omega) = \frac{\mu'\varphi}{-j\omega}\left[1-(1+j)\frac{\delta'}{\Lambda'}\right] \tag{26}$$

where $\delta' = \sqrt{2\mu'/\omega}$ is the thermal skin depth, and Λ' is the thermal characteristic length. Similar to the case of dynamic viscous permeability, with the above two limit conditions satisfied, the dynamic thermal permeability in the medium frequency range can be fitted as [18]:

$$k'(\omega) = \frac{k_0'}{\sqrt{1-j\frac{M'\omega k_0'}{2\mu'\varphi}} - j\frac{\omega k_0'}{\mu'\varphi}} \tag{27}$$

where $M' = (8k_0')/(\varphi\Lambda'^2)$ is the dimensionless thermal shape factor. The static thermal permeability k_0' is a theoretically introduced parameter, which cannot be obtained by experimental measurements. For porous materials, it is proposed that the dimensionless thermal shape factor M' can be approximately taken as 1 [14].

The equivalent bulk modulus of a porous material is defined as:

$$\widetilde{K}(\omega) = K/\beta(\omega) \tag{28}$$

Equation (23) can thence be rewritten as:

$$\frac{1}{\widetilde{K}(\omega)}\frac{\partial\langle p\rangle}{\partial t} = -\nabla\cdot\langle \mathbf{u}\rangle \tag{29}$$

The compression response of air is given by:

$$\frac{1}{K}\frac{\partial\langle p\rangle}{\partial t} = -\nabla\cdot\langle \mathbf{u}\rangle \tag{30}$$

Equations (29) and (30) have the same form. Substitution of (24) and (27) into (28) leads to:

$$\widetilde{K}(\omega) = \frac{\gamma P_0}{\gamma-(\gamma-1)\left[1-j\frac{8\kappa}{\Lambda'^2 C_p\rho_0\omega}\sqrt{1+j\frac{\Lambda'^2 C_p\rho_0\omega}{16\kappa}}\right]^{-1}} \tag{31}$$

Equations (21) and (31) constitute the well-known Johnson-Champoux-Allard (JCA) model for sound propagation in porous materials, the core idea of which is to decouple the viscous and thermal effects of air within the theory of linear acoustics [13,14]. The remaining four parameters in Eqs. (21) and (31), namely, viscous permeability k_0, tortuosity α_∞, viscous characteristic length Λ and thermal characteristic length Λ', are key transport parameters of a porous material, which are calculated by the analytical and numerical method in the following study for both woven and non-crimp fabrics.

2.3. Analytical modelling of transport parameters

The equivalent fluid model of porous materials detailed in the previous section involves several transport parameters that require determination by considering specific morphologies at pore scale. Often, to simplify the analysis, the pores are taken as tortuous capillary tubes. For fully developed laminar flow in a capillary tube, its average velocity u_c is determined by the applied pressure drop Δp over an effective distance L_c, as:

$$u_c = \frac{r_h^2}{c\mu}\frac{\Delta p}{L_c} \tag{32}$$

where r_h is the hydraulic radius of the tube, and c is a constant, equal to 2 if the capillary is circular. By modelling the porous material as a bundle of tortuous capillary tubes distributed in a solid matrix, the average velocity u is given by Ref. [19]:

$$u = u_c\varphi\frac{L}{L_c} = \frac{r_h^2\varphi}{c\mu}\frac{\Delta p}{L_c}\frac{L}{L_c} = \frac{r_h^2\varphi}{c\mu}\frac{\Delta p}{L}\left(\frac{L}{L_c}\right)^2 = \frac{k_0}{\mu}\frac{\Delta p}{L} \tag{33}$$

where L is the thickness of the porous material.

According to the Darcy's law, the average flow velocity of fluid in a porous material is directly proportional to pressure gradient:

$$u = \frac{k_0}{\mu}\frac{\Delta p}{L} \tag{34}$$

where k_0 is the viscous permeability characterizing the capacity of a porous material to conduct fluid, given by:

$$k_0 = \frac{r_h^2 \varphi}{c}\left(\frac{L}{L_c}\right)^2 \tag{35}$$

Here, in the specific case of fabrics, either woven or non-crimp, the hydraulic radius r_h is calculated by:

$$r_h = \frac{V_a}{S} = \frac{V_s \varphi}{(1-\varphi)S} = \frac{d\varphi}{4(1-\varphi)} \tag{36}$$

Substituting Eq. (36) into Eq. (35) leads to:

$$k_0 = \frac{d^2\varphi^3}{16C(1-\varphi)^2} \tag{37}$$

where $C = c(L_c/L)^2$ is the so-called Kozeny-Carman constant.

The tortuosity α_∞ describes the dispersion of fluid velocity caused by variation in pore morphology along the direction of flow. In the extreme case when $\varphi = 1$, the fluid flow is subjected to no disturbance, and hence $\alpha_\infty = 1$. With the limit $\lim_{\varphi\to 1}\alpha_\infty = 1$ satisfied, several empirical functions have been proposed to establish a relationship between the tortuosity and porosity [20–22]. The simplest is the linear expression:

$$\alpha_\infty = 1 + p(1-\varphi) \tag{38}$$

where p is an adjustable parameter.

The viscous characteristic length Λ is related to the viscous dissipation of a sound wave at medium and high frequencies. Upon determining the viscous permeability and tortuosity, the viscous characteristic length can be calculated by Ref. [18]:

$$\Lambda = \sqrt{\frac{8\alpha_\infty k_0}{M\varphi}} \tag{39}$$

where M is the dimensionless viscous shape factor. Substituting (37) and (38) into (39) leads to:

$$\Lambda = d\sqrt{\frac{[1+p(1-\varphi)]\varphi^2}{2MC(1-\varphi)^2}} \tag{40}$$

Similarly, the thermal characteristic length Λ' is used to characterize the thermal dissipation of a sound wave at medium and high frequencies [14], given by:

$$\Lambda' = 2\frac{V_a}{S} = 2\frac{V_s\varphi/(1-\varphi)}{S} = \frac{d\varphi}{2(1-\varphi)} \tag{41}$$

In the theoretical model, C, p and M are three unknown control coefficients, which can be fitted according to numerical and experimental results. Strictly speaking, these control coefficients are closely related to the geometrical configuration of representative unit cell, and remain fixed only when the representative unit cell is scaled up or down. When the geometrical parameters of a fabric are changed, its pore morphology is still square when viewed from top to bottom. As a result, the three control coefficients vary slightly and can be approximated as constants. The theoretical model then shows that the transport parameters of the fabric, either woven or non-crimped, are only related to its fiber diameter and porosity. The viscous permeability is proportional to the square of fiber diameter, while the viscous and thermal characteristic lengths are proportional to fiber diameter. In contrast, the tortuosity has nothing to do with fiber diameter.

Fundamentally, the pore morphology of both woven and non-crimp fabrics is determined by the fiber diameter and porosity (or fiber spacing), thus transport parameters of fabrics can be written as functions of fiber diameter and porosity. According to Taylor's series theorem, the functions of transport parameters can be expanded into polynomial series. The more terms retained in the polynomial series, the more accurate the fitted expression of transport parameters is. However, excessive unknown coefficients increase the workload of expression fitting, and require a large number of numerical calculation results as a reference. In addition, the polynomial expansion series of the transport parameters has no obvious physical meaning, and it is impossible to intuitively see the relationship between transport parameters.

2.4. Sound absorption coefficient

The characteristic impedance Z and the wavenumber k of the equivalent fluid are calculated by:

$$Z = \sqrt{\widetilde{\rho}(\omega)\widetilde{K}(\omega)} \tag{42}$$

$$k = \omega\sqrt{\frac{\widetilde{\rho}(\omega)}{\widetilde{K}(\omega)}} \tag{43}$$

Backed by a rigid wall, the surface impedance of the fabric is given by:

$$z_s = -jZ\cot(kh)/(\varphi Z_0) \tag{44}$$

where h is the total thickness of the fabric, $Z_0 = \rho_0 c_0$ is the characteristic impedance of air, and c_0 is the sound speed in air.

The sound absorption coefficient of the fabric at normal incidence is defined as the ratio of acoustic energy absorbed by it to incident acoustic energy, as:

$$\alpha = 1 - \left|\frac{z_s - 1}{z_s + 1}\right|^2 = \frac{4\mathrm{Re}(z_s)}{[1+\mathrm{Re}(z_s)]^2 + [\mathrm{Im}(z_s)]^2} \tag{45}$$

All the involved thermo-physical parameters of air are listed in Table 1.

3. Numerical model

3.1. Numerical calculation of transport parameters

For periodic porous materials such as micro-lattices [17], packed spherical beads [23], open-cell foams [24] and micro-slit plates [25], the multi-scale asymptotic method has been proved to be effective for calculating relevant transport parameters.

In the limit when the frequency of sound approaches zero, the inertial effects of fluid become negligible and the flow of air is dominated by its viscosity. In this case, the velocity of air can be linked to pressure gradient via the viscous permeability vector $\mathbf{k}$, and the governing equation and boundary conditions are [23]:

$$\nabla^2\mathbf{k} = \nabla q_0 - \mathbf{e} \quad \text{in } \Omega_f \tag{46}$$

Table 1
Thermo-physical parameters of air at ambient temperature (298.15 K).

Thermo-physical parameters	Symbol	Unit	Value
Density	ρ_0	$\mathrm{kg\cdot m^{-3}}$	1.1840
Sound speed	c_0	m/s	346.30
Viscosity coefficient	η	$10^{-6}\mathrm{Pa\cdot s}$	18.490
Specific heat ratio	γ	1	1.4018
Ambient pressure	P_0	kPa	101.325
Specific heat per unit mass	c_p	$10^3\mathrm{J/(kg\cdot K)}$	1.0066
Thermal conductivity	κ	$10^{-3}\mathrm{W/(m\cdot K)}$	25.853

$$\nabla \cdot \mathbf{k} = 0 \quad \text{in } \Omega_f \tag{47}$$

$$\mathbf{k} = \mathbf{0} \quad \text{on} \partial\Omega_{sf} \tag{48}$$

where q_0 is the scaled pressure, $\mathbf{e}$ is the unit vector denoting the applied pressure gradient along the propagating direction of sound, Ω_f is the fluid domain, and $\partial\Omega_{sf}$ represents the solid-fluid interfaces. The macroscopic viscous permeability k_0 of a porous material (woven fabric) is calculated by:

$$k_0 = \varphi\langle k' \rangle \tag{49}$$

where k' is the component of $\mathbf{k}$ along the direction of $\mathbf{e}$, and $\langle\ \rangle$is the average operator over the fluid domain.

In the high frequency limit ($\omega \to \infty$), the viscous skin depth $\delta = \sqrt{2\mu/(\rho_0\omega)}$ becomes so small that the effect of fluid viscosity can be ignored. In this case, the flow of an incompressible perfect fluid through the fabric is analogical to the electrical problem wherein a conductive fluid transports in the porous material with an insulating solid frame. Accordingly, under the external excitation of a unit electric field $\mathbf{e}'$, the local electrical field $\mathbf{E}$ is expressed as:

$$\mathbf{E} = \mathbf{e}' - \nabla q \tag{50}$$

where q is the unknown electrical potential. The divergence of $\mathbf{E}$ is zero, and the insulating boundary condition is applied on the interfaces $\partial\Omega_{sf}$, yielding [23]:

$$\nabla \cdot \mathbf{E} = 0 \ \text{ in } \Omega_f \tag{51}$$

$$\mathbf{E} \cdot \mathbf{n} = 0 \ \text{ on} \partial\Omega_{sf} \tag{52}$$

where $\mathbf{n}$ is the vector normal to solid-fluid interfaces $\partial\Omega_{sf}$. The tortuosity α_∞, the viscous characteristic length Λ, and the thermal characteristic length Λ' are calculated by:

$$\alpha_\infty = \frac{\langle \mathbf{E}\cdot\mathbf{E} \rangle}{\langle \mathbf{E} \rangle \cdot \langle \mathbf{E} \rangle} \tag{53}$$

$$\Lambda = 2\frac{\int_{\Omega_f} \mathbf{E}\cdot\mathbf{E}\mathrm{d}V}{\int_{\partial\Omega_{sf}} \mathbf{E}\cdot\mathbf{E}\mathrm{d}S} \tag{54}$$

$$\Lambda' = 2\frac{\int_{\Omega_f} \mathrm{d}V}{\int_{\partial\Omega_{sf}} \mathrm{d}S} \tag{55}$$

In the Creep Flow module of the commercially available finite element software COMSOL Multiphysics, the viscosity and density of fluid are set to 1 Pa·s and 1 kg·m^{-3}, respectively, and hence the governing equation of fluid flow has the same form as Eq. (46). Upon giving the pressure at the inlet and outlet, the pressure gradient $\mathbf{e}$ is applied. The electrical problem is solved in the Electrostatics module of COMSOL Multiphysics. Similarly, the electric field $\mathbf{e}'$ is applied by setting the electric potential at the inlet and outlet.

3.2. Validation of numerical model

To validate the present numerical model, the sound absorption behavior of a 3D printed micro-lattice reported in a previous study [17] is simulated. The cylindrical specimen of micro-lattice employed for sound absorption experiment [17] is composed of orthogonal parallel circular rods, as shown in Fig. 4. The height and diameter of the specimen are 30 mm, the diameter of each rod is 0.4 mm, and the in-plane spacing between adjacent rods is 0.8 mm. The distance between two consecutive layers is 0.6 mm.

By adopting the multi-scale asymptotic method, the predicted transport parameters of the micro-lattice are listed in Table 2, while its sound absorption coefficient is plotted as a function of frequency in

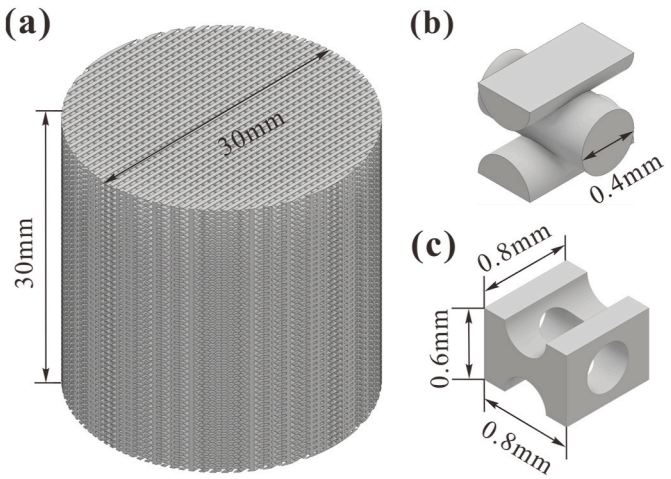

Fig. 4. 3D printed micro-lattice [17]: (a) cylindrical sample for sound absorption measurement; (b) representative unit cell; (c) computational fluid domain.

Table 2
Transport parameters of micro-lattice.

Transport parameters	φ	α_∞	Λ/mm	Λ'/mm	$k_0/(10^{-3}\mathrm{mm}^2)$
Simulation	0.5026	1.2745	0.2171	0.2516	3.0219
Reference [17]	0.51	1.28	0.217	0.252	2.89

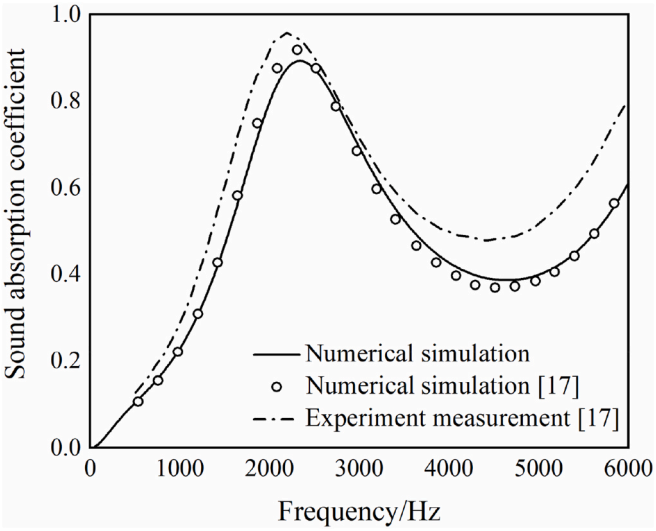

Fig. 5. Sound absorption coefficient of micro-lattice plotted as a function of frequency: comparison between experimental measurements [17] and numerical simulations.

Fig. 5. The prediction results of the present numerical model are consistent with those of the literature [17], thus demonstrating the validity of the present numerical model. The small discrepancy between numerical predictions and experimental measurements mainly stems from various processing defects, such as elliptical rod section, section shrinkage and surface irregularities, as shown in Fig. 6.

4. Transport parameters of woven fabrics

To fit the C, p and M parameters of the analytical model, the transport parameters of a set of woven and non-crimp fabrics are numerically calculated. The fiber diameter is fixed at 1 mm, while the fiber spacing

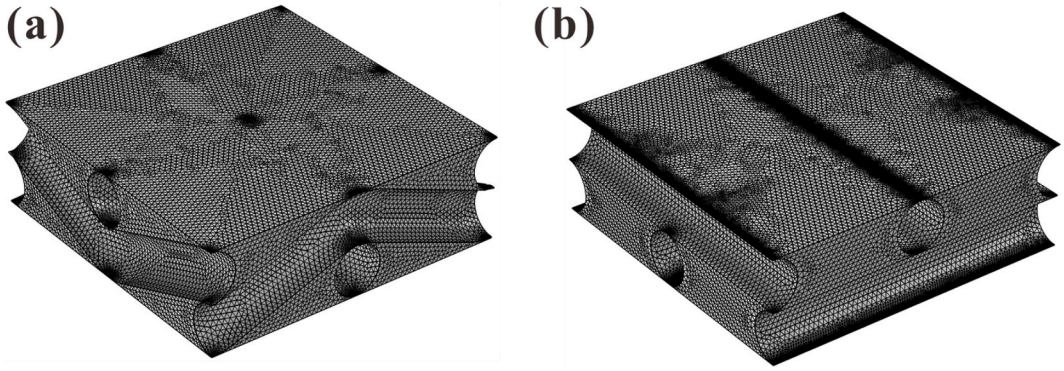

Fig. 6. The numerical simulation domain of (a) woven and (b) non-crimp fabrics.

takes different values to change the porosity of woven fabrics. Fig. 6(a) and (b) present the numerical computational air domain for woven and non-crimp fabrics, respectively, with fiber diameter equal to 1 mm and fiber spacing set to 3 mm. For both woven and non-crimp fabrics, the point contact between adjacent fibers causes singularities during the process of meshing. Since the transport parameters are averaged over the fluid domain of representative unit cell, slightly reducing the fiber diameter to form an air gap instead of point contacts between fibers has a negligible impact on numerical results [26] but can circumvent the singularity. In the present study, the fiber diameter in the numerical model is set to be 99% of its original size.

In Fig. 7, the analytically calculated transport parameters of both woven and non-crimp fabrics are compared with those calculated numerically. Excellent agreement is achieved, thus demonstrating the accuracy of the proposed analytical model. Based on these results for woven fabrics, the Kozeny-Carman constant C, adjustable parameter p, and dimensionless viscous shape factor M are fitted to 2.6751, 0.6078 and 1.4891, respectively. Consequently, the viscous permeability k_0, the tortuosity α_∞, and the viscous characteristic length Λ presented in Eqs. (37), (38) and (40) for woven fabrics can be explicitly expressed as functions of fiber diameter d and porosity φ:

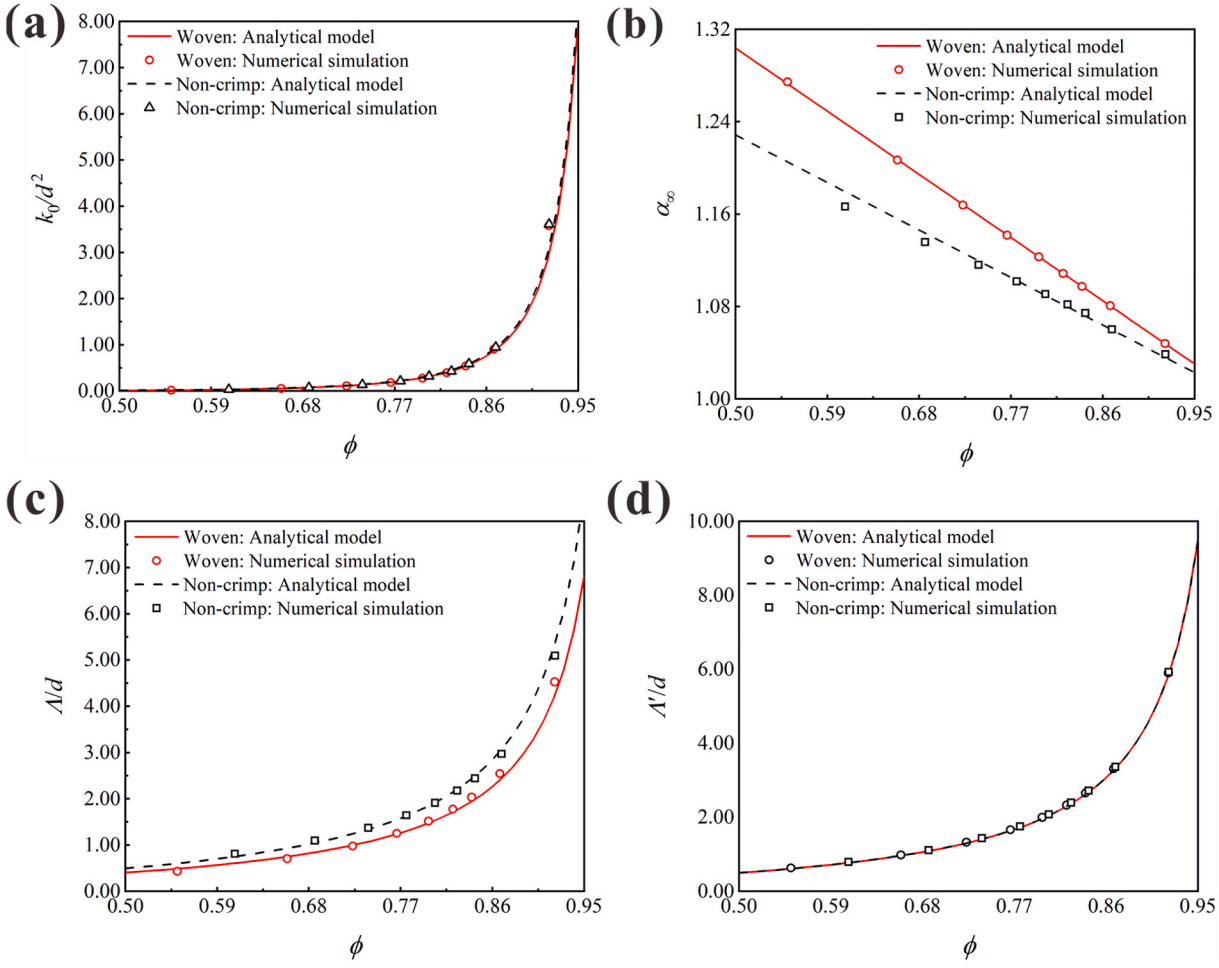

Fig. 7. Normalized transport parameters plotted as function of porosity for both woven and non-crimp fabrics: comparison between analytical calculations and numerical simulations.

$$k_0 = \frac{d^2\varphi^3}{42.8016(1-\varphi)^2} \tag{56}$$

$$\alpha_\infty = 1.6078 - 0.6078\varphi \tag{57}$$

$$\Lambda = d\sqrt{\frac{[1.6078 - 0.6078\varphi]\varphi^2}{7.9670(1-\varphi)^2}} \tag{58}$$

Similarly, for non-crimp fabrics, the parameters are fitted to be 2.5507, 0.4572 and 0.9712, and hence the viscous permeability k_0, tortuosity α_∞ and viscous characteristic length Λcan be explicitly expressed as:

$$k_0 = \frac{d^2\varphi^3}{40.8112(1-\varphi)^2} \tag{59}$$

$$\alpha_\infty = 1.4572 - 0.4572\varphi \tag{60}$$

$$\Lambda = d\sqrt{\frac{[1.4572 - 0.4572\varphi]\varphi^2}{4.9545(1-\varphi)^2}} \tag{61}$$

For both woven and non-crimp fabrics, the viscous characteristic length Λ' is analytically expressed by Eq. (41).

With fixed porosity and fiber diameter, the results of Fig. 8 demonstrate that the permeability and thermal characteristic length of woven fabrics are almost unchanged relative to idealized non-crimp fabrics, while the tortuosity is enlarged and the viscous characteristic length is reduced. This reflects that the disturbance of pore wall to fluid flow is increased after the fibers are woven, causing intensified velocity dispersion and viscous dissipation.

5. Influence of key morphological parameters on sound absorption of woven fabrics

In this section, the validated theoretical model is employed to quantify the effects of several key morphological parameters on sound absorption of woven fabrics, including fiber diameter, porosity and sheet thickness.

5.1. Fiber diameter

The influence of fiber diameter on sound absorption of woven fabric sheets backed by rigid wall is presented in Fig. 8, with the porosity fixed at 0.6 and sheet thickness at 30 mm. For comparison, the results for non-crimp fabrics are also included. As the fiber diameter is increased, the sound absorption of both woven and non-crimp fabrics is seen to firstly increase, reach a peak, and then gradually decrease. This is because, at fixed porosity, fiber spacing and interconnected pores of the fabric are enlarged by increasing the fiber diameter. When the interconnected pores are too small, the large flow resistance makes it hard for a sound wave to enter the fabric and hence the fabric absorbs little sound. In contrast, if the pores are too large, the sound easily passes through the fabric, with little viscous-thermal dissipation of its energy. Consequently, with the porosity fixed, there must exist an optimal pore size (or, equivalently, optimal fiber diameter) such that the energy of sound is dissipated favorably within viscous/thermal boundary layers on fiber surfaces, leading to maximal sound absorption of the fabric. For the parameters chosen here, the optimal fiber diameter appears to be ~0.2 mm, whether the fabric is plain woven or non-crimp. In an earlier study [27], the present authors demonstrated that the optimal pore size for a porous material to absorb sound lies within the sub-millimeter range, affected somewhat by frequency, porosity and other factors (e.g., randomness in pore size/shape, waviness of pore, gradient distribution of pore/porosity, roughness of pore surface, rigidity of solid skeleton, thickness).

From an overall perspective, with identical geometric parameters, the sound absorption performance of woven fabrics is seen from Fig. 8 to be slightly better than that of non-crimp fabrics.

5.2. Porosity

The influence of porosity on sound absorption is quantified, as shown in Fig. 9. In this case, the thickness of fabric sheet thickness is fixed at 30 mm while the fiber diameter is set to 0.1 mm. The results of Fig. 9 reveal that, once fiber diameter (and sheet thickness) are given, excessively reducing or increasing the porosity would deteriorate the sound absorption performance of both woven and non-crimp fabrics. The reason lies in the fact that, at a fixed fiber diameter, fiber spacing and interconnected pores are positively correlated to porosity, and hence the interconnected pores need to have appropriate sizes to ensure optimal performance of the fabric. The physical mechanism is similar to that previously discussed regarding the influence of fiber diameter.

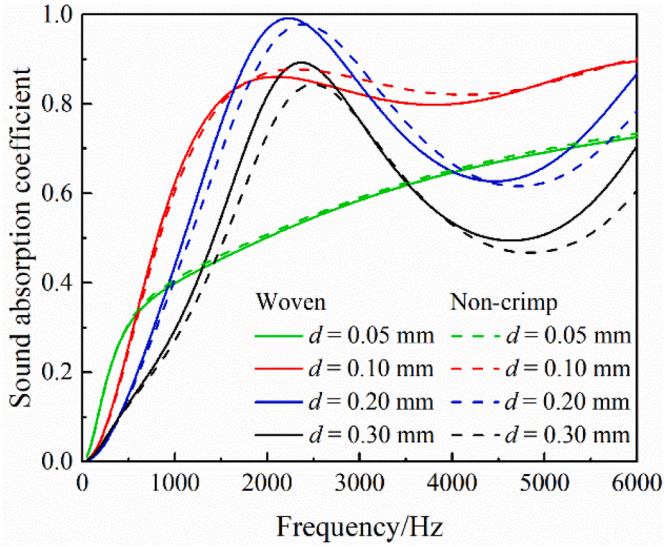

Fig. 8. Influence of fiber diameter on sound absorption versus frequency curves of woven and non-crimp fabric sheets backed by rigid wall (porosity: 0.6; sheet thickness: 30 mm).

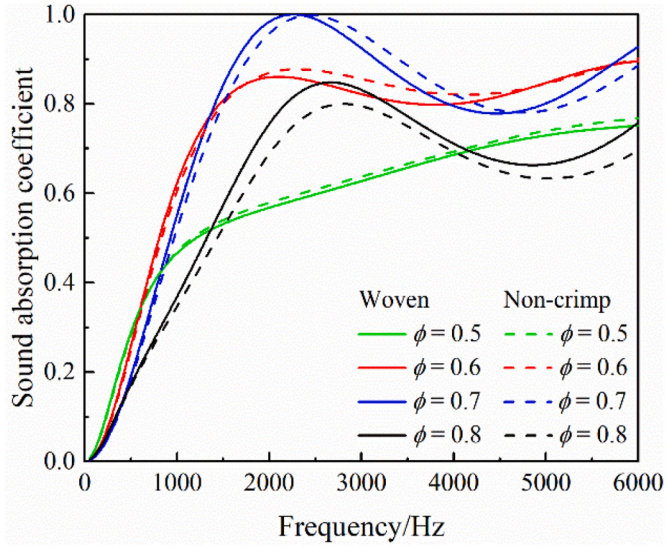

Fig. 9. Influence of porosity on sound absorption versus frequency curves of woven and non-crimp fabric sheets backed by rigid wall (sheet thickness: 30 mm; fiber diameter: 0.1 mm).

5.3. Influence of fiber diameter and porosity on average sound absorption

With the thickness of a woven fabric sheet fixed at 30 mm, Fig. 10 reveals how porosity and fiber diameter affect its sound absorption coefficient averaged within the frequency range of 50 Hz–6000 Hz. Again, for all the calculations, the fabric is backed by a rigid wall. When the porosity is increased and fiber diameter is simultaneously decreased, the sound absorption performance of the woven fabric is enhanced, moving towards the lower right of Fig. 10. However, it is worth emphasizing that rigid fiber skeletons have been assumed in both the theoretical and numerical models of the present study. When the fibers are sufficiently slender and the stiffness of fiber material is relatively low, the fiber skeleton will deform and vibrate under the excitation of incident sound, particularly when sound intensity is high. Under such conditions, the propagation of sound in the woven fabric must account for the effect of fluid-solid coupling, which needs to be explored in future studies.

5.4. Fabric thickness

Finally, the influence of woven fabric sheet thickness on sound absorption is presented in Fig. 11 for fixed fiber diameter (0.1 mm) and porosity (0.6). With the increase of sheet thickness, the propagation path of sound wave is extended and the sound absorption versus frequency curve is shifted towards lower frequencies. However, the marginal benefit of increasing the thickness of the woven fabric to enhance its sound absorption gradually diminishes. The sound absorption of thicker woven fabrics is not necessarily better at all frequencies, especially at medium and high frequencies. The fiber diameter, porosity, and thickness of a woven fabric comprehensively determine its final sound absorption performance. It should also be noted that, for a fixed thickness, there exists an optimal set of fiber diameter and porosity for a certain sound absorption target, e.g., maximum/minimum absorption at a given frequency/frequency range. By embedding the analytical model of sound absorption into the optimization algorithm, the sound absorption of fabrics can reach the expected optimal state.

6. Concluding remarks

An analytical model has been developed to describe the transport parameters and sound absorption performance of woven fabrics having idealized periodic morphologies. The intensity of incident linear harmonic sound wave is relatively low so that the solid skeleton of a woven fabric can be approximately taken as rigid. The analytical model enables linking explicitly the transport parameters of the idealized woven fabric to its fiber diameter and open porosity. The unknown control coefficients of the model are fitted according to numerical simulation results obtained on basis of representative unit cell selected for the fabric. Subsequently, based on the Johnson-Champoux-Allard (JCA) model of porous media, the transport parameters are employed to calculate the sound absorption performance of woven fabrics and quantify the influence of key morphological parameters. For fabrics made by other selected manufacturing processes, the analytical model of transport parameters and sound absorption coefficient should be modified accordingly. It is demonstrated that, with the porosity and fiber diameter fixed, the viscous permeability and thermal characteristic length of a woven fabric remain almost the same as those of an idealized non-crimp fabric, but the tortuosity is enlarged and the viscous characteristic length is reduced. The sound absorption performance of a woven fabric is completely determined by its fiber diameter, porosity, and thickness. Compared with non-crimp fabrics, woven fabrics exhibit slightly superior performance in sound absorption. High porosity woven fabrics with characteristic pore sizes lying in submillimeter range are preferred for optimal sound absorption. The present results provide valuable theoretical guidance for the morphology design of fabrics according to actual noise environment.

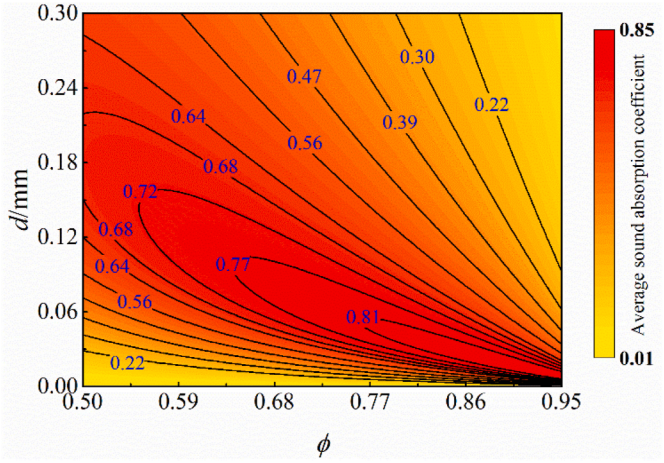

Fig. 10. Influence of porosity and fiber diameter on sound absorption coefficient averaged within the range of 50 Hz–6000 Hz for woven fabric sheet backed by rigid wall, with a fixed sheet thickness of 30 mm.

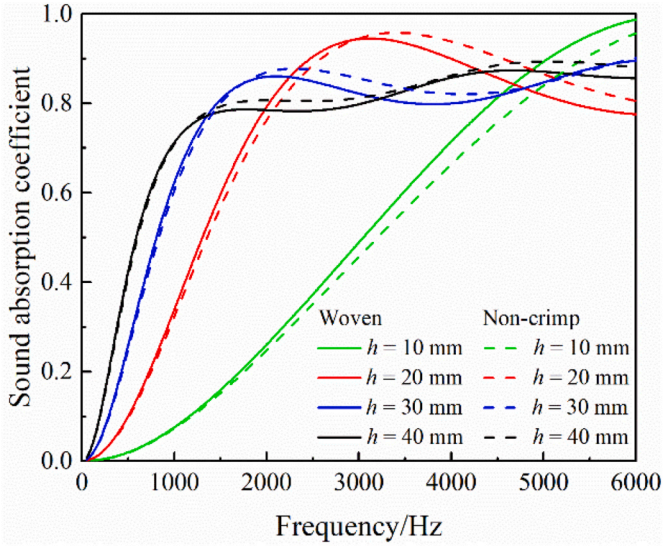

Fig. 11. Influence of sheet thickness on sound absorption versus frequency curve of woven fabric sheet backed by rigid wall (fiber diameter: 0.1 mm; porosity: 0.6).

Author statement

Wei He: Conceptualization, Investigation, Methodology, Software, Formal analysis, and Writing-Original Draft. Xiangjun Peng: Investigation, Software, Validation and Formal analysis. Fengxian Xin: Investigation, Formal analysis, Supervision and Funding Acquisition. Tian Jian Lu: Conceptualization, Methodology, Formal analysis, Writing - Review & Editing, Supervision and Funding Acquisition.

Declaration of competing interest

The authors declare that they have no known competing financial interests or personal relationships that could have appeared to influence the work reported in this paper.

Acknowledgements

This work was supported by the National Natural Science Foundation of China (52075416, 11772248, 11972185and 12032010).

References

[1] M.J. King, P. Jearanaisilawong, S. Socrate, A continuum constitutive model for the mechanical behavior of woven fabrics, Int. J. Solid Struct. 42 (13) (2005) 3867–3896.

[2] E.M. Parsons, M.J. King, S. Socrate, Modeling yarn slip in woven fabric at the continuum level: simulations of ballistic impact, J. Mech. Phys. Solid. 61 (1) (2013) 265–292.

[3] K.R. Hart, P.X.L. Chia, L.E. Sheridan, E.D. Wetzel, N.R. Sottos, S.R. White, Mechanisms and characterization of impact damage in 2D and 3D woven fiber-reinforced composites, Compos. Appl. Sci. Manuf. 101 (2017) 432–443.

[4] M. Grasso, Y. Xu, A. Ramji, G. Zhou, A. Chrysanthou, G. Haritos, Y. Chen, Low-velocity impact behaviour of woven laminate plates with fire retardant resin, Compos. B Eng. 171 (2019) 1–8.

[5] A. Sasikumar, D. Trias, J. Costa, N. Blanco, J. Orr, P. Linde, Impact and compression after impact response in thin laminates of spread-tow woven and non-crimp fabrics, Compos. Struct. 215 (2019) 432–445.

[6] J. Tian, T.J. Lu, H.P. Hodson, D.T. Queheillalt, H.N.G. Wadley, Cross flow heat exchange of textile cellular metal core sandwich panels, Int. J. Heat Mass Tran. 50 (13–14) (2007) 2521–2536.

[7] J. Xu, J. Tian, T.J. Lu, H.P. Hodson, On the thermal performance of wire-screen meshes as heat exchanger material, Int. J. Heat Mass Tran. 50 (5–6) (2007) 1141–1154.

[8] S.C. Costa, H. Barrutia, J.A. Esnaola, M. Tutar, Numerical study of the pressure drop phenomena in wound woven wire matrix of a Stirling regenerator, Energy Convers. Manag. 67 (2013) 57–65.

[9] G. Zhu, Y. Fang, L. Zhao, J. Wang, W. Chen, Prediction of structural parameters and air permeability of cotton woven fabric, Textil. Res. J. 88 (14) (2017) 1650–1659.

[10] B. Yin, Y. Wen, T. Hong, Z. Xie, G. Yuan, Q. Ji, H. Jia, Highly stretchable, ultrasensitive, and wearable strain sensors based on facilely prepared reduced graphene oxide woven fabrics in an ethanol flame, ACS Appl. Mater. Interfaces 9 (37) (2017) 32054–32064.

[11] R. Pieren, K. Heutschi, Predicting sound absorption coefficients of lightweight multilayer curtains using the equivalent circuit method, Appl. Acoust. 92 (2015) 27–41.

[12] X. Tang, D. Kong, X. Yan, Multiple regression analysis of a woven fabric sound absorber, Textil. Res. J. 89 (5) (2018) 855–866.

[13] D.L. Johnson, J. Koplik, R. Dashen, Theory of dynamic permeability and tortuosity in fluid-saturated porous media, J. Fluid Mech. 176 (1987) 379–402.

[14] Y. Champoux, J.F. Allard, Dynamic tortuosity and bulk modulus in air-saturated porous media, J. Appl. Phys. 70 (4) (1991) 1975–1979.

[15] I. Prasetiyo, E. Muqowi, A. Putra, M. Novenbrianty, G. Desendra, D.R. Adhika, Modelling sound absorption of tunable double layer woven fabrics, Appl. Acoust. 157 (2020), 107008.

[16] Z. Cai, X. Li, X. Gai, B. Zhang, T. Xing, An empirical model to predict sound absorption ability of woven fabrics, Appl. Acoust. 170 (2020), 107483.

[17] J. Boulvert, J. Costa-Baptista, T. Cavalieri, M. Perna, E.R. Fotsing, V. Romero-García, G. Gabard, A. Ross, J. Mardjono, J.-P. Groby, Acoustic modeling of micro-lattices obtained by additive manufacturing, Appl. Acoust. 164 (2020), 107244.

[18] D. Lafarge, P. Lemarinier, J.F. Allard, V. Tarnow, Dynamic compressibility of air in porous structures at audible frequencies, J. Acoust. Soc. Am. 102 (4) (1997) 1995–2006.

[19] P.C. Carman, Flow of Gases through the Porous Medium, Butterworths Scientifc Publications, London, 1956.

[20] M. Barrande, R. Bouchet, R. Denoyel, Tortuosity of porous particles, Anal. Chem. 79 (2007) 9115–9121.

[21] M.M. Ahmadi, S. Mohammadi, A.N. Hayati, Analytical derivation of tortuosity and permeability of monosized spheres: a volume averaging approach, Phys. Rev. 83 (2) (2011), 026312.

[22] Z. Sun, X. Tang, G. Cheng, Numerical simulation for tortuosity of porous media, Microporous Mesoporous Mater. 173 (2013) 37–42.

[23] T.G. Zieliński, Microstructure-based calculations and experimental results for sound absorbing porous layers of randomly packed rigid spherical beads, J. Appl. Phys. 116 (3) (2014), 034905.

[24] C. Perrot, F. Chevillotte, M. Tan Hoang, G. Bonnet, F.-X. Bécot, L. Gautron, A. Duval, Microstructure, transport, and acoustic properties of open-cell foam samples: experiments and three-dimensional numerical simulations, J. Appl. Phys. 111 (1) (2012), 014911.

[25] T.G. Zieliński, F. Chevillotte, E. Deckers, Sound absorption of plates with micro-slits backed with air cavities: analytical estimations, numerical calculations and experimental validations, Appl. Acoust. 146 (2019) 261–279.

[26] S.I. Green, Z. Wang, T. Waung, A. Vakil, Simulation of the flow through woven fabrics, Comput. Fluid 37 (9) (2008) 1148–1156.

[27] X. Wang, T.J. Lu, Optimized acoustic properties of cellular solids, J. Acoust. Soc. Am. 106 (2) (1999) 756–765.